Curcumin partly ameliorates irinotecan-induced diarrhea and synergistically promotes apoptosis in colorectal cancer through mediating oxidative stress

Da-Jian Zhu[1,2,*], Yan-Feng Huang[3,*], Xiao-Wu Chen[1], Zhen-Tao Luo[1], Guo-Xin Wang[1], Chang-Chun Liu[1], Wei-Jie Zhang[1], Man-Zhao Ouyang[1]

[1]Department of Gastrointestinal Surgery, Shunde First People's Hospital Affiliated to Southern Medical University, Guangdong 528300, China

[2]Department of Gastrointestinal Surgery, Shunde Women and Children's Hospital Affiliated to Jinan University, Guangdong 528300, China

[3]Department of Traditional Chinese Medicine, Shunde First People's Hospital Affiliated to Southern Medical University, Guangdong 528300, China

[*]These authors have contributed equally to this work

Correspondence to: *Xiao-Wu Chen,* ***email:*** *drchenxiaowu@163.com*

Keywords: *curcumin, colorectal cancer, irinotecan, diarrhea, oxidative stress*

Received: *December 07, 2015* ***Accepted:*** *May 12, 2016* ***Published:*** *July 14, 2016*

ABSTRACT

OBJECTIVE: Development of treatment resistance and adverse toxicity limits the gains made by irinotecan in patients with colorectal cancer. According to our previous studies, we found that curcumin could enhance the efficacy of irinotecan-induced apoptosis of colorectal tumor cells in vitro. This study aims to examine the effectiveness of a combination treatment regimen of irinotecan and curcumin in the colorectal cancer xenograft model.

RESULTS: Curcumin or irinotecan alone reduced the tumor volume, and the combination had the strongest anticancer effects. Oxidative stress was induced in tumor (MDA: $P < 0.01$, GPx: $P < 0.05$, PRDX4: $P < 0.01$), while was reduced in intestinal tissue (MDA: $P < 0.01$, SOD: $P < 0.05$, GPx: $P < 0.01$). The apoptosis in tumor was accompanied by up-regulation of apoptotic proteins (caspase-3: $P < 0.01$, Bax: $P < 0.01$), but down-regulation of anti-apoptotic proteins (pro-caspase-3: $P < 0.01$, Bcl-2: $P < 0.01$). Besides, the combination treatment alleviated diarrhea and intestine injury, and also restored the autophagy (PGC-1α: $P < 0.05$, Atg-7: $P < 0.05$, and LC3B: $P < 0.05$) and mitochondrial dynamics (Mfn-1: $P < 0.01$, Mfn-2: $P < 0.01$, Drp-1: $P < 0.01$, Fis-1: $P < 0.05$) in intestinal tissue.

MATERIALS AND METHODS: Nude mice were implanted with LoVo colorectal cancer cells before randomization into the following treatment groups: control; curcumin only; irinotecan only; curcumin + irinotecan. After a 9-day treatment, we compared the tumor weight, tumor volume, morphological change of intestine, and oxidative stress factors (LDH, MDA, SOD, GPx). In addition, we detected the oxidative stress (PRDX4, MnSOD, and p53), apoptosis (Bax, Bcl-2, pro-caspase-3, cleaved-caspase-3) and autophagy (PGC-1α, Atg-7, and LC3B) signaling.

CONCLUSIONS: Curcumin could enhance the efficacy of irinotecan-induced apoptosis of colorectal cancer in vivo, while restore the irinotecan-induced autophagy of small intestinal epithelium.

INTRODUCTION

Colorectal cancer (CRC) is the second most prevalent cancer, with more than 1.2 million new cancer cases and over 600,000 deaths per year [1]. 8% of cancer related deaths in men and 9% in women are caused by colorectal cancer [2]. The current management of unresectable metastatic CRC consists of systemic chemotherapy

involving various agents. Irinotecan is extensively used in first and second line treatment for unresectable and metastatic disease of colorectal cancer [3]. Combined chemotherapies of irinotecan with other drugs improve the median survival of patients with metastatic CRC. However, chemoresistance and toxicity are two major issues that hamper the success of irinotecan-based chemotherapies, as well as other current standard tumor chemotherapies. Combined therapy of agents with different mechanisms of action is a feasible and effective means to minimize the side effects and avoid the resistance to chemotherapeutic drugs while improving the antitumor effects.

Irinotecan functions as a topoisomerase-I-inhibitor in cancer cells, which interrupts DNA replication and finally causes cell death. High exposure to irinotecan and its active metaboliteSN-38 could lead to adverse drug events, including severe diarrhea, deep myelosuppression, vomiting, fatigue and even death [4–6]. Pervious study reported that irinotecan generates high levels of oxidative stress in cells [7], which could cause cell dysfunction and unpredictable toxicities, including the apoptosis of small intestine epithelium.

Curcumin (diferuloylmethane, $C_{21}H_{20}O_6$) is derived from the medical plant *Curcuma longa*, which has well-known pharmacologic activities, especially anti-tumor, anti-oxidation, and anti-inflammatory properties [8–10]. Curcumin was reported to have anti-cancer effects in diverse cancers [11–16], including colorectal cancer [17, 18]. The related mechanisms involve apoptosis inducement, cell cycle arrest, and inhibition of cell proliferation and invasion. Also, curcumin was reported to have benefit effect on rapid and complete resolution of HIV related-diarrhea [19].

According to our previous study [20], we found that curcumin could enhance the efficacy of irinotecan-induced apoptosis of colorectal cancer LoVo cell. We also identifed the proteins associated with this property by MALDI-TOF/TOF. The results indicated that the combination of curcumin and irinotecan mainly activate intracellular calcium pathways, cellular respiratory chain pathway and intracellular redox reaction pathways in vitro.

In the current study, we investigated the synergistic anti-tumor effect of combination of curcumin and irinotecan against colorectal cancer in vivo. During the study, we found that curcumin could inhibit cancer cell growth and notably remit the symptom of irinotecan-related diarrhea. In this article, the possible mechanisms focusing on oxidative stress-mediated apoptosis in tumor and autophagy in intestine will be illustrated.

RESULTS

Combination of curcumin with irinotecan effectively suppress colorectal cancer in vivo

Throughout the experiment, the body weight of the animals was unaffected by any of the treatments (by curcumin and/or irinotecan) (Figure 1A). The average tumor volumes of CUR and IRI group animals were both significantly lower than the vehicle treated animals throughout the study (Figure 1B), indicating that both curcumin and irinotecan treatments suppressed tumor growth compared with the control group. The combinatorial administration of with curcumin and irinotecan further attenuated tumor growth, indicating that combined treatment was significantly more effective than either agent alone. Meanwhile, significant decrease of tumor weight (Figure 1C) was observed in the treated groups, compared to the control group. Especially, average tumor weight of CUR+IRI group was significantly lower than the IRI or CUR groups.

Figure 2 showed plasma concentrations vs. time curves of irinotecan and SN-38 following the last administration, alone or with orally curcumin supplement. In plasma, Tmax of irinotecan were observed 2 h after last administration of irinotecan for both groups; curcumin does not affect the time required for the plasma concentration to reach its maximum value. There was no significantly difference of concentrations of irinotecan and SN-38 between the 2 groups at all the 4 time points (Figure 2A, 2B). In intestinal tissue, concentrations of irinotecan and SN-38 were not significantly different between both groups either (Figure 2C, $P > 0.05$).

Effect of curcumin on oxidative stress in tumor

As shown in Figure 3, exposure to the irinotecan led to an increase in LDH and MDA levels in serum in comparison with the control group ($P < 0.05$, and $P < 0.05$, respectively). The effects were partially blocked by curcumin supplement ($P < 0.05$, and $P < 0.01$, respectively) (Figure 3G, 3H). By contrast, exposure to the irinotecan led to a decrease in SOD and GPx levels in serum ($P < 0.05$, and $P < 0.01$, respectively). Notably, all these effects were blocked by curcumin supplement ($P < 0.01$ and $P < 0.01$, respectively) (Figure 3I, 3J). On the other hand, different results were shown in xenograft tissue. MDA level was increased in CUR+IRI group much more compared to IRI group ($P < 0.01$, Figure 3A). Both SOD and GPx levels were decreased by irinotecan treatment ($P < 0.01$, and $P < 0.01$, respectively Figure 3B, 3C), and combinational treatment decreased GPx levels much more than irinotecan treatment ($P < 0.05$, Figure 3C). Besides, we examined PRDX4 protein which indicatives of oxidative status. Western blot analysis (Figure 4D, 4E) and immunohistochemical (Figure 5) revealed that both IRI and CUR+IRI treatments could decrease the expression PRDX4. These results indicated that combinational management might accelerate oxidative stress in tumor.

Combination of curcumin with irinotecan suppresses tumor growth through inducing apoptosis

It was shown that both irinotecan and curcumin could increase the number of TUNEL-positive cells

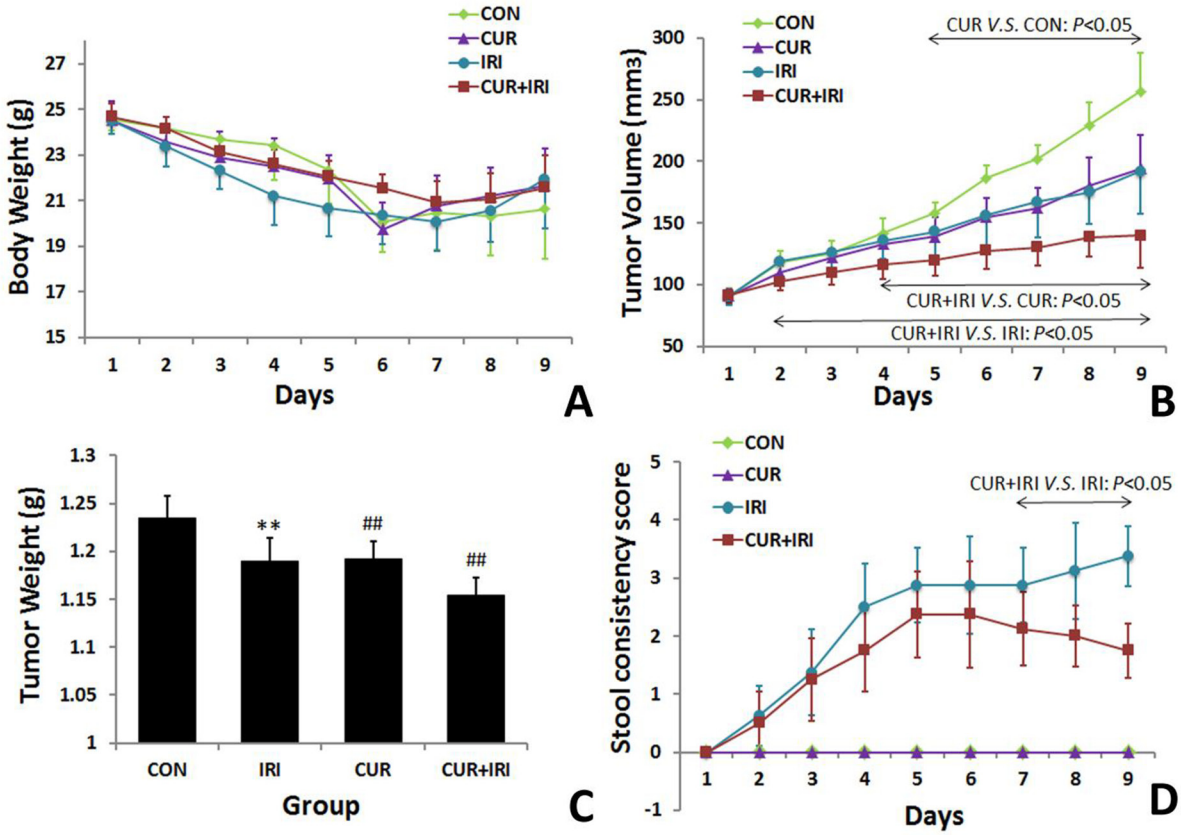

Figure 1: Effects of irinotecan and/or curcumin treatment on general condition. 1×10^6 LoVo cells were subcutaneously injected into BALB/c-nude mice. After the tumor was established, the mice were treated with irinotecan and/or curcumin, tumor volume, body weight and severity of diarrhea were recorded, followed by measuring of tumor weight on the 10th day when mice were sacrificed. **A.** Changes of body weight during the whole period. **B.** Effects of irinotecan and curcumin treatments on tumor volume. **C.** Effects of irinotecan and curcumin treatments on tumor weight. **D.** Effects of irinotecan and/or curcumin treatments on stool. Data are represented as means ± SEM. **, $P < 0.01$ vs. CON group; ##, $P < 0.01$ vs. IRI group.

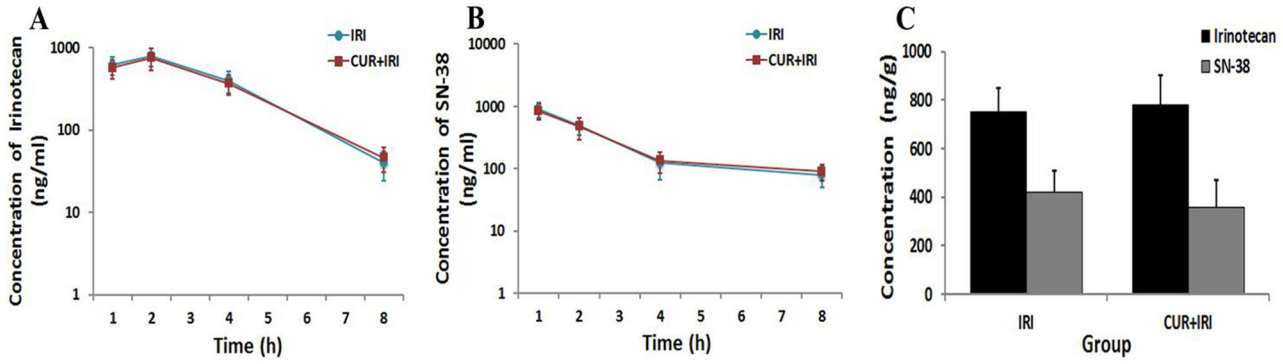

Figure 2: Irinotecan and SN-38 concentrations in plasma and intestinal tissue. Blood samples were withdrawn at 1, 2, 4 and 8 h after the last irinotecan administration, and the intestinal tissues were collected 8 h after the last irinotecan administration. Irinotecan and SN-38 concentrations of samples were quantified using the HPLC with fluorescence detector. **A.** Irinotecan plasma concentrations after the last administration of irinotecan either given alone or with curcumin (n=3 mice for each time). **B.** SN-38 plasma concentrations after the last administration of irinotecan either given alone or with curcumin (n=3 mice for each time). **C.** Irinotecan and SN-38 concentrations in intestinal tissue 8 h after the last administration of irinotecan either given alone or with curcumin (n=3 per group). Data are represented as means ± SEM.

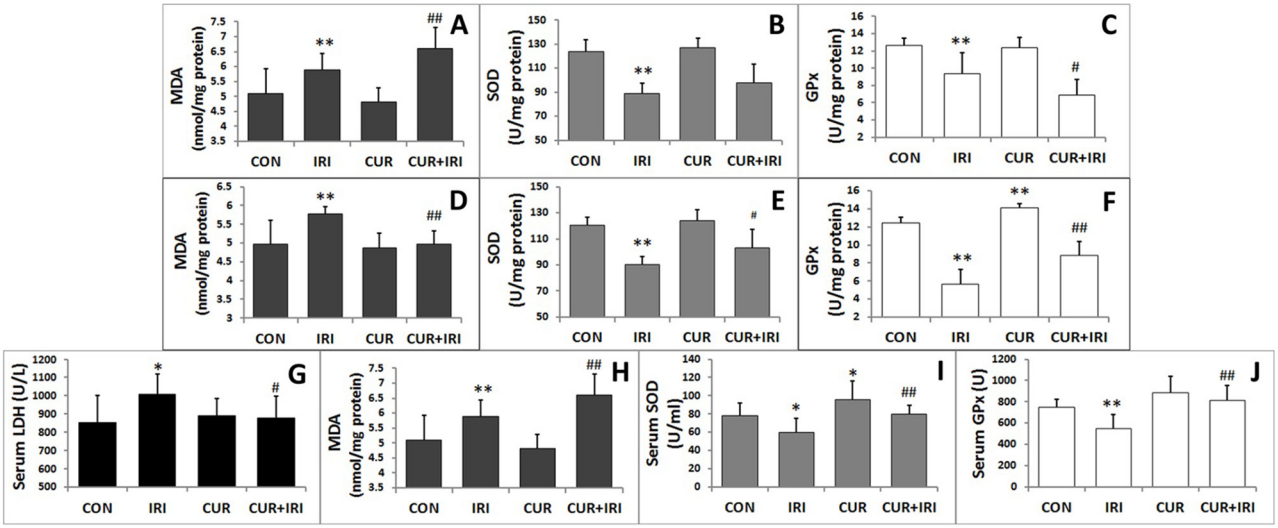

Figure 3: Biochemical parameters of oxidative stress in tissues and serum. A. MDA level of tumor tissue. **B.** SOD level of tumor tissue. **C.** GPx level of tumor tissue. **D.** MDA level of intestinal tissue. **E.** SOD level of intestinal tissue. **F.** GPx level of intestinal tissue. **G.** Serum LDH level. **H.** Serum MDA level. **I.** Serum SOD level. **J.** Serum GPx level. Data are represented as means ± SEM. *, $P < 0.05$ vs. CON group; **, $P < 0.01$ vs. CON group; #, $P < 0.05$ vs. IRI group; ##, $P < 0.01$ vs. IRI group.

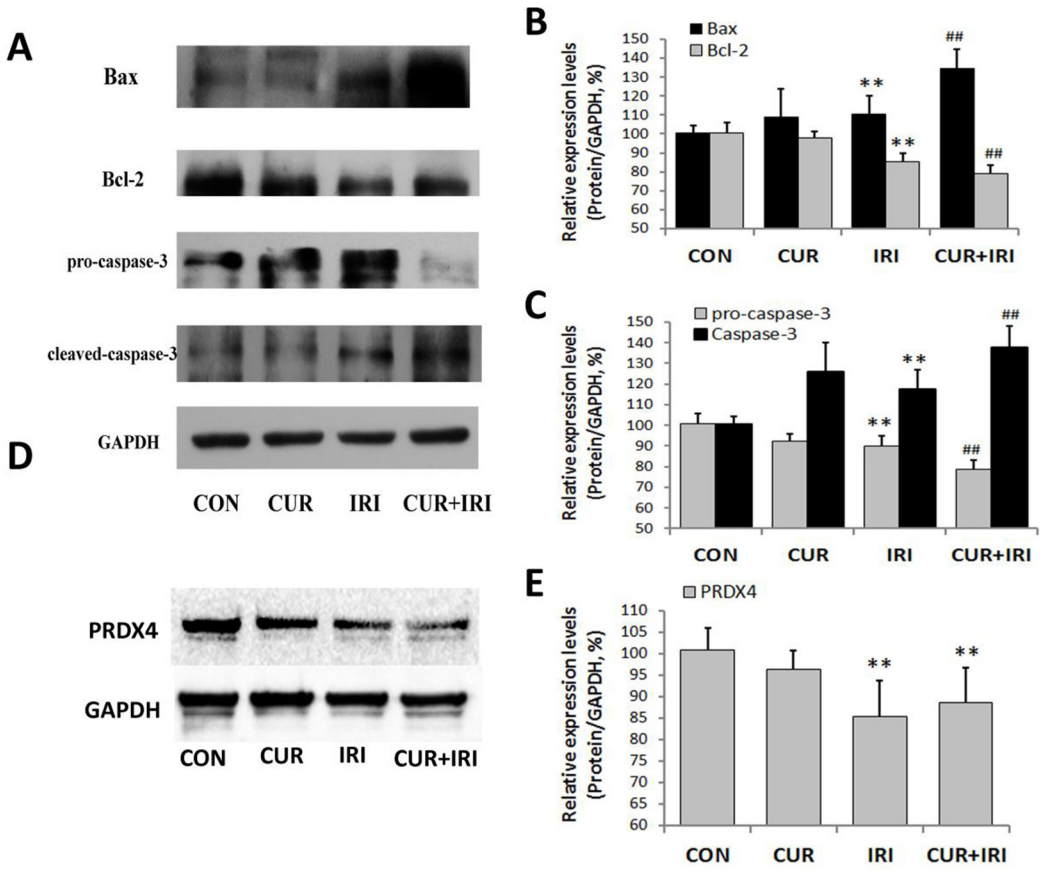

Figure 4: Effects of irinotecan and/or curcumin treatment on apoptosis and oxidative stress in tumor. Expression of apoptosis related proteins Bax, Bcl-2, pro-caspase-3 and cleaved-caspased-3, and oxidative stress related protein PRDX4 were determined by western blotting in tumor tissues. GAPDH was used as internal control. **A, B, C.** Protein levels of Bax, Bcl-2, pro-caspase-3 and cleaved-caspased-3 (A, Western blot images; B, C, statistical results); **D, E.** Protein levels of PRDX4 (D, Western blot images; E, statistical results). Data are represented as means ± SEM. **, $P < 0.01$ vs. CON group; ##, $P < 0.01$ vs. IRI group.

($P < 0.01$, $P < 0.01$), and combinational management could increase much more ($P < 0.01$, $P < 0.01$) (Figure 6). As shown in Figure 4, compared with that in the control group, the proapoptotic protein Bax was markedly induced in all the treatment groups, whereas Bcl-2 was significantly inhibited, indicating that the apoptotic effects of curcumin may be partly mediated by upregulating the Bax/Bcl-2 protein ratio, a critical determinant of apoptosis. Additionally, the other two important signal molecules, caspase-3 and pro-caspase-3, were also assessed. Statistical analysis revealed that the expression levels of caspase-3 in treatment groups were significantly increased. And the expression of pro-caspase-3 was decreased in CUR and CUR+IRI groups compared with that in control group. Both the expression levels of caspase-3 and pro-caspase-3 in CUR+IRI group were higher, compared with the IRI group ($P < 0.01$, $P < 0.01$) (Figure 4A, 4C).

Curcumin protects against the adverse side-effects of irinotecan

Since day 2 after the first irinotecan injection, 62.5% (5 in 8 mice) of animals in IRI group and 50% (4 in 8 mice) in CUR+IRI suffered from mild diarrhea. Both the

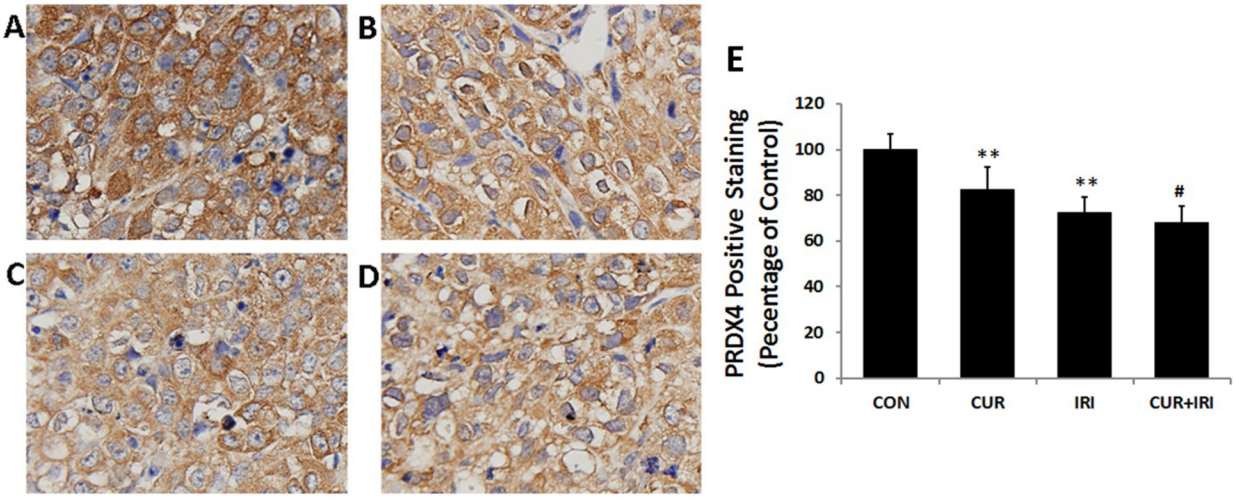

Figure 5: Immunohistochemical staining for PRDX4 (magnification of 400 ×). A. CON group; **B.** CUR group; **C.** IRI group; **D.** CUR+IRI group; **E.** Quantification of PRDX4 staining as relative percentage to control. Data are represented as means ± SEM. **, $P < 0.01$ vs. CON group; #, $P < 0.05$ vs. IRI group.

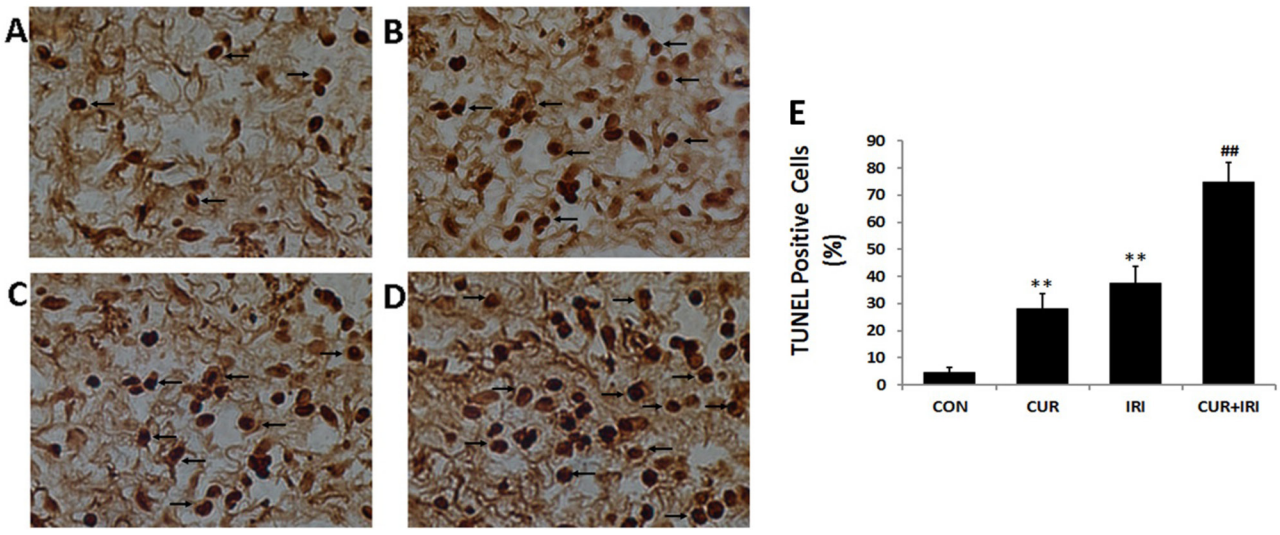

Figure 6: TUNEL staining in tumor tissue (magnification of 400 ×). Cells in brown were positive for TUNEL staining (arrows). **A.** CON group; **B.** CUR group; **C.** IRI group; **D.** CUR+IRI group. **E.** Quantification of the number of TUNEL positive apoptotic cells. Data are represented as means ± SEM. **, $P < 0.01$ vs. CON group; ##, $P < 0.01$ vs. IRI group.

amount and the manifestation gradually increased in the next days and lasted to end point of observation. During the whole experiment, mice in CUR+IRI groups suffered less from diarrhea than the ones in IRI group ($P < 0.001$) (Figure 1D). The mice in CON and CUR groups showed no visible diarrhea.

Figure 7 showed the results of histological examinations. Mice treated with irinotecan suffered from a massive destruction of small intestinal mucosa at both the 2 different time points (8 hours and 10 days after the last irinotecan administration) (Figure 7A, 7D). Pathological changes include villus shortening, massive destruction of epithelial layer, and cellular debris. Only minimal differences of visible signs of inflammation (such as an enhanced infiltration of neutrophils), could be detected between CON and CUR groups (Figure 7C, 7E). On the other hand, samples of mice treated with irinotecan and curcumin showed preservation of the crypts and villi and of the epithelial cell surface (Figure 7F).

Effect of curcumin on oxidative stress in intestine

MDA level was increased in IRI group ($P < 0.01$), which could be restored by curcumin supplement ($P < 0.01$) (Figure 3D). SOD and GPx levels in intestinal tissue were decreased by irinotecan treatment ($P < 0.01$, and $P < 0.01$, respectively), which could both restored by curcumin ($P < 0.05$, and $P < 0.01$, respectively) (Figure 3E, 3F). These results indicated that curcumin could increase antioxidant enzymes activity to ameliorate oxidative stress. Besides, we examined proteins which indicative of oxidative status. Both MnSOD and p53 were increased by irinotecan, which could be inhibited by curcumin supplement (Figure 8A, 8C).

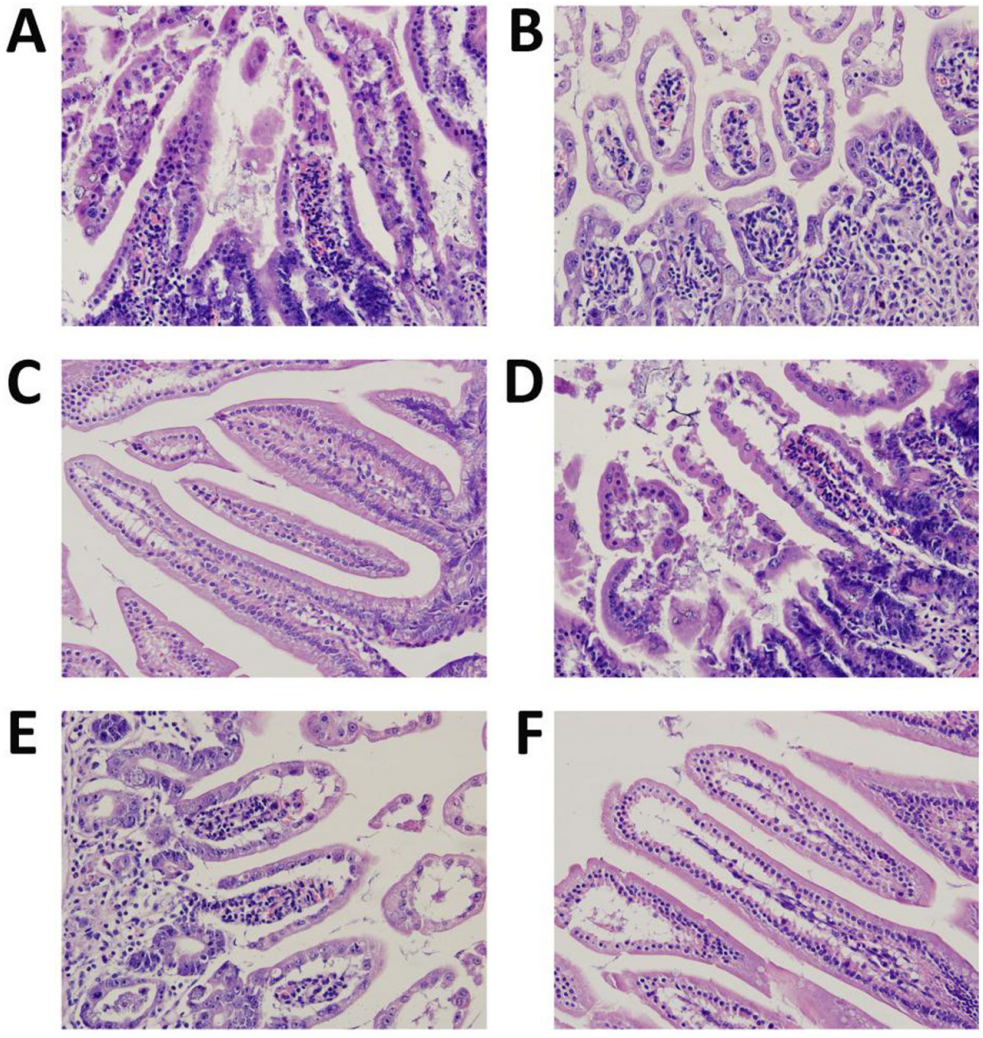

Figure 7: Morphology of the intestines photographed after H&E staining (magnification of 400 ×). A. IRI group, 8 h after the last irinotecan administration (n=12); **B.** CUR+IRI group, 8 h after the last irinotecan administration (n=12); **C.** CON group, mice sacrificed on the 10th day (n=8); **D.** IRI group, mice sacrificed on the 10th day (n=8); **E.** CUR group, mice sacrificed on the 10th day (n=8); **F.** CUR+IRI group, mice sacrificed on the 10th day (n=8).

Effect of curcumin on autophagy and mitochondrial dynamics in intestine

As shown in Figure 9, irinotecan-treatment increased the number of intracellular autophagosomes in intestinal mucous epithelial cells, accompanied by over-expression of Atg7 and LC3B proteins (Atg7: $P < 0.01$, LC3B: $P < 0.01$) (Figure 5D, 5E), the well-known markers of autophagy. Compared with the IRI group, cells from CUR+IRI group exhibited an obvious decrease in the number of intracellular autophagosomes. This decrease was associated with decreased expression of Atg7 and LC3B proteins (Atg7: $P < 0.05$, LC3B: $P < 0.05$) (Figure 5D, 5E).

According to the results of Western blotting, we found that irinotecan decreased PGC-1α (a kind of transcriptional co-activator essential to mitochondrial biosynthesis) expression level ($P < 0.01$), which could be restored by curcumin supplement ($P < 0.05$) (Figure 5A, 5B). It was similar to results of diarrhea assessment of animals. As shown in Table 1, mitochondrial fusion-related genes (Mnf1, Mnf2 and Opa1) presented lower expression in intestinal tissue samples of IRI group compared with CON group, while the mitochondrial fission-related genes (Drp-1 and Fis-1) presented higher. It revealed that mitochondrial fusion was inhibited while fission was stimulated in mice with irinotecan treatment. The changes of Mnf-1, Mnf-2, Drp-1 and Fis-1 could be restored if the IRI mice were treated with curcunmin supplementation. Together, these results suggest that curcumin may inhibit irinotecan-induced autophagy in intestinal mucous epithelial cells by restoring the mitochondrial dynamics.

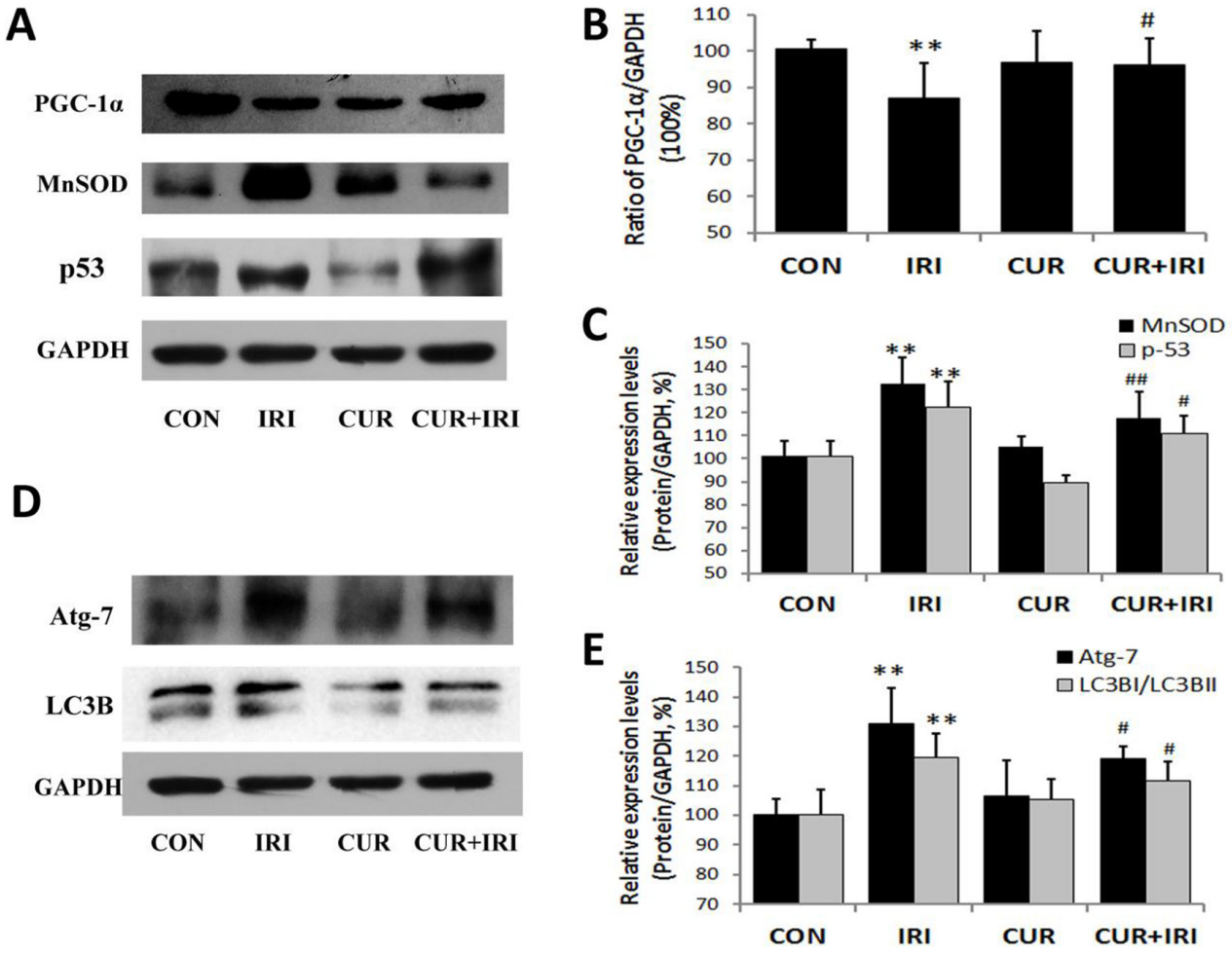

Figure 8: Effects of irinotecan and/or curcumin treatment on mitochondrial biogenesis and autophagy activation. Expression of proteins PGC-1α, MnSOD, p53, Atg-7 and LC3B were determined by western blotting in intestinal tissues. GAPDH was used as internal control. **A, B, C.** Protein levels of PGC-1α, MnSOD and p53 (A, Western blot images; B, C, statistical results); **D, E.** Protein levels of Atg-7 and LC3B (D, Western blot images; E, statistical results). Data are represented as means ± SEM. *, $P < 0.05$ vs. CON group; **, $P < 0.01$ vs. CON group; #, $P < 0.05$ vs. IRI group; ##, $P < 0.01$ vs. IRI group.

DISCUSSION

This study showed, for the first time, the synergetic effect of curcumin and irinotecan on colorectal cancer, and the amelioration effect of curcumin on irinotecan-induced diarrhea in xenograft model. We demonstrated that curcumin supplementation potentiates the antitumor effects of irinotecan in treatment of colorectal cancer via apoptosis activation. The severity of irinotecan related-diarrhea might correlate with the accumulation of reactive oxygen species (ROS), and the curcumin restores intestinal epithelial cell (IEC) damage and mitochondria dysfunction.

It has been proved that curcumin could enhance the anti-tumor efficacy of the chemotherapeutic agents (such as celecoxib, phenethyl isothiocyanate, gemcitabine, dasatinib, 5-FU, oxaliplatin) on colorectal cancer cell [21]. The mechanisms involved down-regulation of the epidermal growth factor receptor (EGFR) and insulin-like growth factor 1 receptor (IGF-1R), and miRNA-induced suppression of epithelial-to-mesenchymal transition (EMT) as well [24–26]. Previously, we reported that curcumin could enhance the efficacy of irinotecan-induced apoptosis colorectal cancer LoVo cells in vitro [20]. We also performed preliminary experiment of curcumin dose in vivo, which showed that high dose (1,000mg/kg, daily, 15 days) curcumin oral administration remarkably inhibited growth of the xenograft tumors than low-dose (250mg/kg, daily, 15 days) or medium-dose (500mg/kg, daily, 15 days), without adverse side-effects (Supplement 1). In this study, we demonstrated that the combination of curcumin with irinotecan markedly inhibited the growth in vivo, and investigated the possible underlying mechanism.

By determinating irinotecan and SN-38 concentrations of plasma and intestinal tissue, we found no significant differences between animals in IRI group and CUR+IRI group, which indicated that the effects of irinotecan are unimpaired in curcumin-treated animals. Tumor volume and tumor weight revealed that curcumin and/or irinotecan treatments could strongly inhibit the growth of fully established LoVo tumor xenografts. Especially, the combinatorial treatment significantly suppressed the tumor growth without nonspecific toxicity, compared with the IRI and CUR groups.

PRDX4 contributes to cell survival by anti-oxidant activity against ROS. Reducing PRDX4 expression significantly decreased tumor cell growth due to the increased levels of ROS, DNA damage, and apoptosis [22]. In our study, results of biochemical

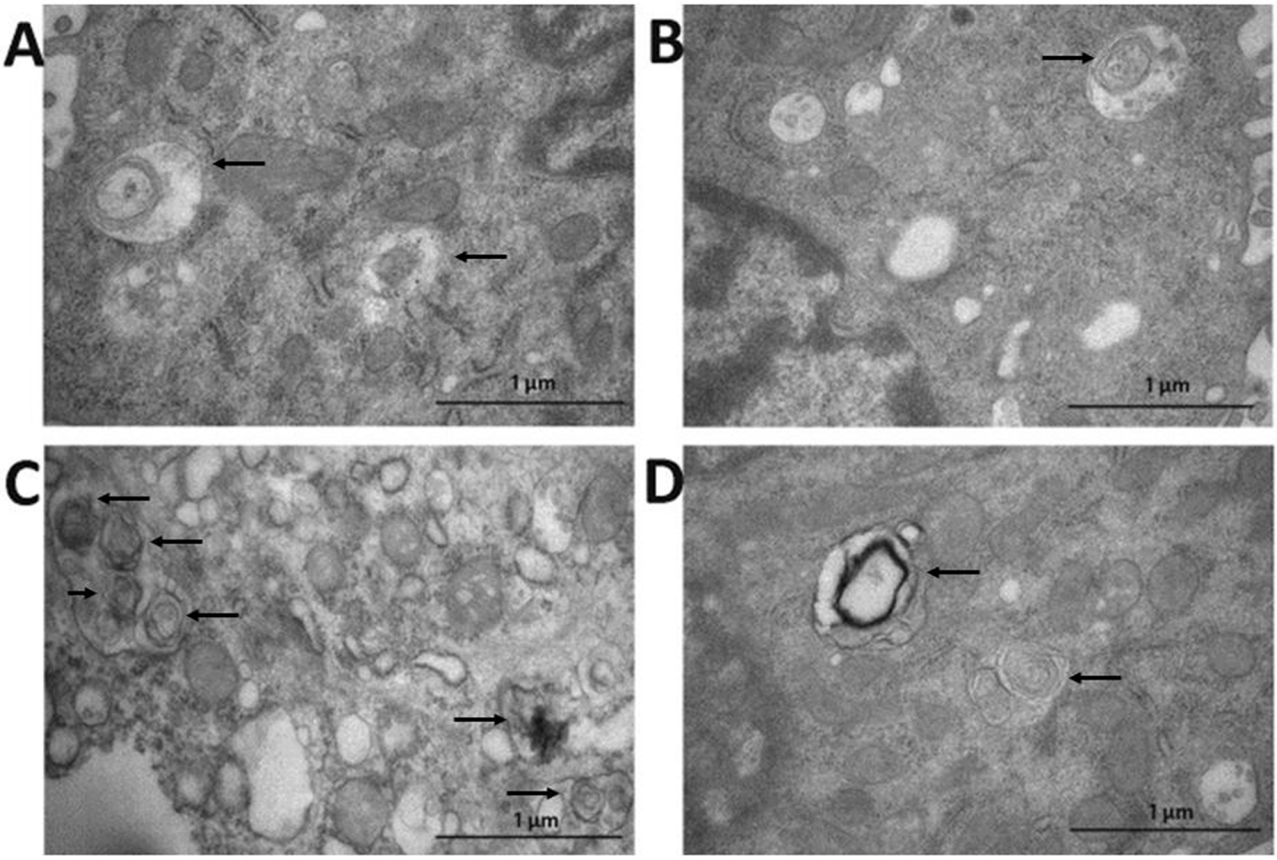

Figure 9: Detection of autophagosome in intestinal tissue by transmission electron microscope (arrows). A. CON group; **B.** CUR group; **C.** IRI group; **D.** CUR+IRI group.

Table 1: Fusion and fission-related genes mRNA expression

	CON	IRI	CUR	CUR+IRI
Mfn-1	1.000	0.596 ± 0.036**	1.156 ± 0.117**	0.962 ± 0.280##
Mfn-2	1.000	0.691 ± 0.258**	1.045 ± 0.086	0.907 ± 0.067##
Opa-1	1.000	0.843 ± 0.151**	1.024 ± 0.115	0.748 ± 0.245
Drp-1	1.000	2.456 ± 0.264**	0.959 ± 0.286	1.724 ± 0.098##
Fis-1	1.000	1.514 ± 0.464**	1.001 ± 0.258	1.118 ± 0.218#

**, $P < 0.01$ vs. CON group; #, $P < 0.05$ vs. IRI group; ##, $P < 0.01$ vs. IRI group.

parameters of enhanced oxidative stress revealed that combinational management of curcumin and irinotecan accelerated oxidative stress much more than irinotecan treatment. What's more, PRDX4 levels were significantly decreased in IRI and CUR+IRI groups, which might be a potential mechanism for the suppression of tumor growth in mice with curcumin supplementation.

Apoptosis is a programmed cell death and is a key target in the development of anti-cancer therapies. Anticancer drugs can also block the cell cycle and inhibit cell growth, while activating caspase cascades and modulating telomerase expression and activity [23–25]. In this study, both the curcumin and combinatorial treatment could provoke apoptosis in vivo. In addition, combinatorial treatment significantly increased expression of pro-apoptotic Bax protein in tumors rather than irinotecan treatment, while decreased the anti-apoptotic protein Bcl-2. The apoptosis induction of LoVo tumor xenografts also involved activation of caspase-3 and down-regulation of pro-caspase-3. Caspase-3 is pivotal in cell apoptosis. The expression of caspase-3 was enhanced with the combinatorial treatment, which proved that the combination stimulates the activation of the apoptotic machinery. Our findings are consistent with studies in small cell lung cancer [26, 27] and leukemia [28].

Patients treated with irinotecan suffer from severe late diarrhea, which prevents irinotecan dose intensification and compromises efficacy. The exact mechanism of irinotecan-induced late diarrhea is not totally clear. But it is suggested that exposure to high concentrations of SN-38 produces characteristic mucosal changes in the intestine by inducing apoptosis and cell differentiation [29, 30]. The underlying mechanism might be associated with high levels of oxidative stress and inflammation generated by irinotecan. In this study, we established a LoVo tumor xenografts model to learn more about mechanism of irinotecan-induced diarrhea. Results of H&E staining revealed that irinotecan resulted in severe small intestinal mucosa damage morphologically, which could be ameliorated by curcumin supplementation. The result of biochemical parameters in serum and in intestinal tissue showed that irinotecan could induce high ROS production, which is consistent with previous reports [7, 31]. The increase levels of MnSOD and p53 in intestinal tissues further determined. We hypothesized that oxidative stress causes by irinotecan could induce mucosal damage, and finally leads to late diarrhea.

Since mitochondria are a major source of ROS in cells, we focused on mitochondrial dynamics in our study. Mitochondrial quality control process included mitogenesis and mitophagy. Mitochondrial perturbations caused by oxidative stress have been intimately linked to autophagy/mitophagy. Removal of damaged mitochondria by mitophagy is critical for maintaining mitochondrial quality control [32] and cellular homeostasis [33]. Peroxisome proliferator-activated receptor gamma co-activator 1 (PGC-1) is a superfamily of transcriptional co-activators which are important precursors to mitochondrial biosynthesis. According to the result, irinotecan decreased PGC-1α level in intestinal tissue. Also, the autophagy markers Atg7 and LC3 were highly induced by irinotecan. Thus, we concluded that irinotecan treatment may inhibit PGC-1α expressin and trigger activation of mitophagy. In addition, mitochondrial dynamics are restored by coordinated fusion and fission processes [34], and derangements in fusion-fission could cause the formation of dysfunctional aberrant mitochondria [35]. The result of qRT-PCR showed that fusion-related genes (Mfn-1, Mfn-2 and Opa-1) were decresed in the intestinal tissue, while fission-related genes (Drp-1 and Fis-1) were increased, which revealed derangements in mitochondrial fusion-fission.

Curcumin has been applied to clinical therapy due to its effectiveness and few side effects. Curcumin could protect mitochondria by scavenging ROS, inhibiting mitochondrial swelling, increasing the activities of antioxidant enzymes, and ameliorating mitochondrial dysfunction ultimately by improving energy metabolism [36–38]. What's more, it has been reported that curcumin could relieve HIV-related diarrhea by decreasing mucosal permeability through mucosal inflammatory pathways [19]. In this study, we demonstrated that curcumin could

ameliorate irinotecan-induced diarrhea by anti-oxidation. Our findings suggested that oxidative stress caused by irinotecan could be restored by curcumin supplementation. The increase of PGC-1α level and the decrease of autophagy markers (Atg7 and LC3) revealed that curcumin could ameliorate mitogenesis and mitophagy in intestinal tissue. In addition, curcumin may promote mitochondrial fusion and inhibit fission, according to the qRT-PCR results. These results were consistent to previous studies which elaborated relationship between mitochondrial dynamics and mitochondria physiology [34, 39].

The findings presented here suggest for the first time that curcumin enhances the efficacy of irinotecan-based chemotherapy in colorectal cancer and relieves the symptoms of irinotecan-related diarrhea in xenograft model. Our results reveal that curcumin could improve oxidative stress damage of intestinal epithelium by restoring mitochondrial dynamics. Besides, combination treatment enhances the efficacy of irinotecan in the LoVo xenograft model. Currently, safe agents which improve the efficacy without increasing side effects in combinatorial regimens are urgently needed in chemotherapy. These findings may demonstrate an accessible combinatorial strategy of colorectal cancer.

MATERIALS AND METHODS

Cell line and cell culture

Colorectal cancer LoVo cells (ATCC, USA) were purchased from the Type Culture Collection of the Chinese Academy of Sciences, Shanghai, China. The LoVo cells were cultured as monolayers in RPMI 1640 medium (Gibco, USA) supplemented with 10% fetal bovine serum (Gibco, Brazil) and 1% penicillin/streptomycin. Cells were grown at 37°C in a humidified atmosphere containing 5% CO_2.

Animals

Specific pathogen-free BALB/c-nude female mice (6 weeks old, 20~22g) were obtained from the Experimental Animal Center of Southern Medical University, China (Approval No. SCXK (Yue) 2011-0015). The mice were housed were housed 4 per cage at a room maintained of 23°C ± 2°C with a 12h-light and 12h-dark cycle (lights on from 7: 00 am to 7: 00 pm) and had *ad libitum* access to food and water. The mice were conducted in accordance with the guidelines of Care and Use of Laboratory Animals formulated by the Ministry of Science and Technology of China, and all experimental procedures concerned were approved by the Animal Ethics Committee of Southern Medical University. All efforts were made to minimize the number of animals used and their suffering.

There was 1-week acclimatization for the mice before the experiments. Xenograft tumors were generated by subcutaneous injection of 1×10^6 LoVo cells (in 0.2 ml phosphate-buffered saline) into the right flank of the mice. Tumor volume was measured with the aid of a ruler and calculated according to the formula: $(\pi/6)$ (length × width^2). Treatment was delivered once the tumor size reached 80~100 mm^3, from day 8 to 10 after cell inoculation. Animals with an accidental death or insufficient tumor development were screened out. Animals were randomly divided into four groups: (i) Control (vehicle, CON group, n=8), (ii) Irinotecan (100 mg/kg daily for 4 consecutive days, IRI group, n=20, 12 of which for irinotecan and SN-38 assay), (iii) Curcumin (1,000 mg/kg daily, CUR group, n=8) or (iv) Curcumin and irinotecan (CUR+IRI group, n=20, 12 of which for irinotecan and SN-38 assay). The irinotecan treatments were injected intraperitoneally 100 mg/kg daily for the first 4 consecutive days. Curcumin was emulsified in a 0.9% saline solution and Tween 20 at a dose of 1,000 mg/kg body weight. Curcumin or the vehicle was administered by oral gavage daily since the first day, for 9 consecutive days. All mice were sacrificed under ether anesthesia with intraperitoneal injection of ketamine (80 mg/kg) and xylazine (4 mg/kg) on the 10th day. Blood samples of the mice were respectively collected in tubes by heart puncture. Tumors and intestinal tissues were collected rapidly under standard conditions. Serum was separated by centrifugation at 3000 rpm at 4°C for 10 min. Tissues were isolated immediately, stored at -80°C until further use.

Animals have been monitored daily during the period. Tumor volume and body weight were measured (as described above) and recorded every day. Severity of diarrhea was scored independently by two experienced researchers according to the stool consistency score (0: normal, 1: loose stool, 2: loose/some diarrhea, 3: diarrhea, 4: severe watery diarrhea) [40]. Before every stool consistency measurement clean white tissues were placed at the bottom of the cage to allow determination of the consistency of the stool. Results are expressed as mean ± SEM.

For irinotecan and SN-38 assay, blood samples (0.5 mL on average) were withdrawn by heart puncture of mice in IRI and CUR+IRI groups (3 mice in each group for each time), and collected in heparinized tubes at 1, 2, 4 and 8 h after the last irinotecan administration. After the last blood sampling, the 24 mice were sacrificed. The intestinal tissues were isolated immediately for concentrations determination.

PRDX4 expression by immunohistochemistry

The tumor samples harvested for histological study were paraffin embedded and serially sectioned

(4μm). Then tissue sections were processed by de-paraffining, rehydrating through an alcohol gradient, peroxidase clearing, antigen retrieval and blocking, antibody binding, 3,3'-diaminobenzidine tetrahydrochloride (DAB) staining, washing with distilled water, hematoxylin staining, niacin alcohol differentiation, dilute ammonia bluing, incremental graded alcohol dehydration, xylene and conventional resin mounting. The primary antibody was rabbit-anti-human PRDX4 monoclonal antibody (1:50, Santa Cruz Biotechnology), and the secondary biotin-labeled antibody was used at 1:200. Streptavidin was labeled with horseradish peroxidase at 1:200 for color development. The Integral Optical Density (IOD) was quantified with Image Pro Plus (at least 3 random fields of each section, 20–30 randomly chosen fields for each group). The index of MOD (IOD /area) was used to reflect the expression of PRDX4.

TdT-mediated dUTP nick-end labeling (TUNEL) assay

Paraffin-embedded sections were stained using the *in situ* apoptosis detection TUNEL kit (Promega, USA) following manufacturer's instructions. Sections were then counter stained with hematoxylin. The results were recorded under light microscope (magnification of 400 ×). The number of TUNEL positive cells in a given visual field was enumerated by manual counting (at least 3 random fields of each section, 20 to 30 randomly chosen fields for each group).

Morphological assessment of intestinal tissues

Intestinal tissues of the 24 mice sacrificed 8h after the last irinotecan-treatment and the rest mice sacrificed on the last day were both performed histological examinations. The isolated intestinal tissues were flushed with PBS, and then were respectively fixed in 10% (v/v) neutral buffered formalin, and then were trimmed, embedded in paraffin, sectioned at 4–6μm thickness using a Leica rotation microtome, finally stained with hematoxylin and eosin (H&E) for histopathological evaluation. Subsequent examination was processed by light microscopy (Nikon Mikrophot-FXA).

The autophagy of intestinal tissues was evaluated by autophagosome screening under transmission electron microscope. The isolated intestinal tissues from the mice sacrificed on the last day were flushed with PBS and fixed in 2.5% glutaraldehyde. Then the specimens were rinsed in 0.1mol/L phosphate buffer. After hydration by graded ethanol, specimens were infiltrated and embedded with epoxy resin. Ultra-thin slices were cut with a diamond knife and then examined with a transmission electron microscope [41].

Determination of irinotecan and SN-38 concentrations in plasma and intestinal tissues

Blood samples were centrifuged for 10 min at 6200 g. Plasma were harvested into clean tubes and immediately analysed as described before [42]. Intestinal tissue were collected and stored at -80°C until analysis. Each weighted intestinal tissue was mixed first with 50μL of acetonitrile and 50μL of water.

Irinotecan and SN-38 plasma concentrations were quantified using a HPLC method coupled with fluorescence detector. Quantification followed solidphase extraction. For analysis, 100μL of plasma was mixed with 200μL of acetonitrile acidified (to 1 mL acetonitrile add 50lL acetic acid). The mixture was vortexed for 10s and centrifuged for 10 min at 5000 rpm. Supernatants were harvested into clean tubes and then evaporated under a gentle stream of nitrogen at 30°C. The residue was reconstituted in acetonitrile/acetic acid mixture (70/30) acidified with trifluoroacetic acid (to 10 mL of mixture add 30 lL trifluoroaceticacid) and vortexed for 20 s. An aliquot of 100μL was then injected into the chromatographic system.

Chromatographic analysis was accomplished using a Nucleosil C18 column (4.6*125mm, 3lm) (Interchim, Montlucon, France) with a mobile phase (acetonitrile/methanol/tetra butyl ammonium 0.0025M pH=3.2, 22/5/73, v/v/v) delivered at a flow rate of 1.2 mL/min. The eluent was monitored at 260 nm. The irinotecan and SN-38 standard curves were correctly described by unweighted least-square linear regression. Over the irinotecan (or SN-38) plasma concentration range of 10~2500 ng/mL (5~1250 ng/mL), the determination coefficient (R^2) of the calibration curves remained > 0.99. Based on quality control samples, the overall relative SD (an index of precision) was less than 12%. The irinotecan and SN-38 lower limits of quantification were 10 and 5 ng/mL. Three irinotecan and SN-38 quality controls were prepared: low (30 and 15 ng/mL), medium (750 and 375 ng/mL) and high (2000 and 1000 ng/mL).

As for intestinal tissue, irinotecan and SN-38 were then extracted according to the extraction protocol as described above [42]. The extraction was repeated four times. Irinotecan and SN-38 tissue concentrations were quantified using the HPLC with fluorescence detector. Calibration standards of irinotecan and SN-38 were prepared in drug-free tissues by spiking with concentrated standards to obtain a concentration range of irinotecan (or SN-38) between 0.5 and 50 ng/g (0.25–25 ng/g). Three irinotecan and SN-38 quality controls were prepared in drug-free tissues by spiking concentrated standards: low (1.5 and 0.75 ng/g), medium (7.5 and 3.75 ng/g) and high (40 and 20 ng/g). Irinotecan and SN-38 lower limit of quantification were 0.5 and 0.25 ng/g.

Biochemical analysis related to oxidative stress

Levels of blood superoxide dismutase (SOD), malondialdehyde (MDA), glutathione peroxidase (GPx) and lactate dehydrogenase (LDH) were determined using commercially available kits from the Jiancheng Bioengineering Institute (Nanjing, China).

Part of the tumor and intestinal tissue samples were homogenized in ice-cold buffer (0.25 M sucrose, 10 mM Tris–HCl, and 0.25 Mm phenylmethylsulfonyl fluoride; pH 7.4), and a portion of the homogenate was measured immediately for malondialdehyde (MDA) levels. Another portion of the homogenate was centrifuged at 15,000g for 30 min at 4°C; the supernatant was decanted and assayed for SOD, GPx activities. The SOD, GPx activities and MDA levels were determined according to the recommended procedures provided by the commercial kits (Jiancheng Bioengineering Institute, Nanjing, China).

Western blotting analyses

Intestinal tissues were lysed with liquid nitrogen and RIPA lysis buffer (Beyotime, Jiangsu, China). The lysates were homogenized and the homogenates were centrifuged at 13,000g for 15 min at 4°C. Proteins were isolated from cultured cells using RIPA lysis buffer following the same protocol. The supernatants were collected and protein concentrations were determined with a BCA Protein Assay kit (Pierce, No. 23225). Equal aliquots (30μg) of protein samples were applied to 10% SDS–PAGE gels, transferred to polyvinylidene fluoride (PVDF) membranes, and blocked with 5% skim milk TBST (Tris-buffered Saline Tween-20) buffer. The membranes were incubated with primary antibodies including anti-PGC-1, anti-MnSOD, anti-p53, anti-pro-caspase-3, anti-PRDX4, anti-GAPDH (1:1000; Santa Cruz Biotechnology); anti-Bax, anti-Bcl-2, anti-caspase-3, anti-Atg7, anti-LC3B (1:1000; Cell Signaling) at 4°C overnight. Then the membranes were incubated with anti-rabbit or anti-mouse antibodies at room temperature for 1 h. The protein bands of LC3B were captured and documented through gel image analysis system (ChemiDox XRS, Bio-Rad, USA); others were exposed by film (Nikon, Japan) in darkroom. The intensities of the protein bands were analyzed by Molecular Imaging Software Version 4.0 which was provided by Kodak 2000 MM System. GADPH protein was used as the internal control.

Quantitative RT-PCR analyses

The total RNA was extracted from the intestinal tissue samples and the administrated cells using the RNAiso Plus reagent (Takara, No. 9108) based on the supplier's protocol, and quantified using a spectrophotometer set at 260 nm. cDNA was synthesized by RT reagent Kit (TaKaRa, No. RR047A) at 37°C for 15 min and at 85°C for 5 s. Quantitative RT-PCR was performed using SYBR PrimeScriot RT-PCR Kit (Takara, No. RR820A) on a Stratagene MX3005P QRT-PCR system (Agilent Technologies, Santa Clara, USA). The primers used in the qRT-PCR reactions were shown in Table 2 . The thermal cycles for PCR amplification were carried out with an initial denaturation at 95°C for 5 min followed by 45 cycles of denaturation (10 s, 95°C), annealing (10 s, 60°C for Drp-1; 60.5°C for Mfn-1, Opa-1 and GAPDH; 61°C for Mfn-2; and 62°C for Fis-1) and extension (12 s, 72°C).

Statistical analyses

Quantitative data are presented as means ± SEM. The data were analyzed by homogeneity test for variance firstly. If the data were homoscedasticity, the significance of the mean difference was determined by one-way ANOVA, followed by a LSD-t test for multigroup comparisons. Otherwise, it was determined by Tamhane's T2 test. All the statistical analyses were performed using SPSS 13.0 statistical software (SPSS, Chicago, IL, USA). A P value < 0.05 was considered statistically significant.

Table 2: Primers and conditions used for RT-PCR

Gene	Forward primer (5'-3'), reverse primer (5'-3')	T-An.(°C)	Gene	Forward primer (5'-3'), reverse primer (5'-3')	T-An. (°C)
Mfn-1	ATGGCAGAAACGGTATCTCCA CTCGGATGCTATTCGATCAAGTT	60.5	Drp-1	CAGGAATTGTTACGGTTCCCTAA CCTGAATTAACTTGTCCCGTGA	60
Mfn-2	CTGGGGACCGGATCTTCTTC CTGCCTCTCGAAATTCTGAAACT	61	Fis-1	TGTCCAAGAGCACGCAATTTG CCTCGCACATACTTTAGAGCCTT	62
Opa-1	TGGAAAATGGTTCGAGAGTCAG CATTCCGTCTCTAGGTTAAAGCG	60.5	GAPDH	TGGATTTGGACGCATTGGTC TTTGCACTGGTACGTGTTGAT	60.5

T-An.: annealing temperature; Mfn-1: mitofusin 1; Mfn-2: mitofusin 2; Opa-1: optic atrophy 1; Drp-1: dynamin-related protein q; Fis-1: mitochondrial fission 1 protein.

CONFLICTS OF INTEREST

The authors declare no conflicts of interest.

REFERENCES

1. Jemal A, Bray F, Center MM, Ferlay J, Ward E, and Forman D. Global cancer statistics. CA. 2011; 61:69-90.
2. Siegel RL, Miller KD, and Jemal A. Cancer statistics, 2015. CA. 2015; 65:5-29.
3. Vanhoefer U, Harstrick A, Achterrath W, Cao S, Seeber S, and Rustum YM. Irinotecan in the treatment of colorectal cancer: clinical overview. Journal of clinical oncology. 2001; 19:1501-1518.
4. Rowinsky EK, Adjei A, Donehower RC, Gore SD, Jones RJ, Burke PJ, Cheng YC, Grochow LB, and Kaufmann SH. Phase I and pharmacodynamic study of the topoisomerase I-inhibitor topotecan in patients with refractory acute leukemia. Journal of clinical oncology. 1994; 12:2193-2203.
5. Ramchandani RP, Wang Y, Booth BP, Ibrahim A, Johnson JR, Rahman A, Mehta M, Innocenti F, Ratain MJ, and Gobburu JV. The role of SN-38 exposure, UGT1A1*28 polymorphism, and baseline bilirubin level in predicting severe irinotecan toxicity. Journal of clinical pharmacology. 2007; 47:78-86.
6. Rothenberg ML. Efficacy and toxicity of irinotecan in patients with colorectal cancer. Seminars in oncology. 1998; 25:39-46.
7. Conklin KA. Chemotherapy-associated oxidative stress: impact on chemotherapeutic effectiveness. Integrative cancer therapies. 2004; 3:294-300.
8. Aggarwal BB, and Harikumar KB. Potential therapeutic effects of curcumin, the anti-inflammatory agent, against neurodegenerative, cardiovascular, pulmonary, metabolic, autoimmune and neoplastic diseases. The international journal of biochemistry & cell biology. 2009; 41:40-59.
9. Odot J, Albert P, Carlier A, Tarpin M, Devy J, and Madoulet C. In vitro and in vivo anti-tumoral effect of curcumin against melanoma cells. International journal of cancer. 2004; 111:381-387.
10. Subramanian M, Sreejayan, Rao MN, Devasagayam TP, and Singh BB. Diminution of singlet oxygen-induced DNA damage by curcumin and related antioxidants. Mutation research. 1994; 311:249-255.
11. Amin AR, Haque A, Rahman MA, Chen ZG, Khuri FR, and Shin DM. Curcumin induces apoptosis of upper aerodigestive tract cancer cells by targeting multiple pathways. PloS one. 2015; 10:e0124218.
12. Jain A, Samykutty A, Jackson C, Browning D, Bollag WB, Thangaraju M, Takahashi S, and Singh SR. Curcumin inhibits PhIP induced cytotoxicity in breast epithelial cells through multiple molecular targets. Cancer letters. 2015; 365:122-131.
13. Seo JA, Kim B, Dhanasekaran DN, Tsang BK, and Song YS. Curcumin induces apoptosis by inhibiting sarco/endoplasmic reticulum Ca(2+) ATPase activity in ovarian cancer cells. Cancer letters. 2016; 371:30-37.
14. Wang J, Zhang J, Zhang CJ, Wong YK, Lim TK, Hua ZC, Liu B, Tannenbaum SR, Shen HM, and Lin Q. In situ Proteomic Profiling of Curcumin Targets in HCT116 Colon Cancer Cell Line. Scientific reports. 2016; 6:22146.
15. Wu GQ, Chai KQ, Zhu XM, Jiang H, Wang X, Xue Q, Zheng AH, Zhou HY, Chen Y, Chen XC, Xiao JY, Ying XH, et al. Anti-cancer effects of curcumin on lung cancer through the inhibition of EZH2 and NOTCH1. Oncotarget. 2016. doi: 10.18632/oncotarget.8532.
16. Zanotto-Filho A, Braganhol E, Klafke K, Figueiro F, Terra SR, Paludo FJ, Morrone M, Bristot IJ, Battastini AM, Forcelini CM, Bishop AJ, Gelain DP, et al. Autophagy inhibition improves the efficacy of curcumin/temozolomide combination therapy in glioblastomas. Cancer letters. 2015; 358:220-231.
17. McFadden RM, Larmonier CB, Shehab KW, Midura-Kiela M, Ramalingam R, Harrison CA, Besselsen DG, Chase JH, Caporaso JG, Jobin C, Ghishan FK, and Kiela PR. The Role of Curcumin in Modulating Colonic Microbiota During Colitis and Colon Cancer Prevention. Inflammatory bowel diseases. 2015; 21:2483-2494.
18. Rajitha B, Belalcazar A, Nagaraju GP, Shaib WL, Snyder JP, Shoji M, Pattnaik S, Alam A, and El-Rayes BF. Inhibition of NF-kappaB translocation by curcumin analogs induces G0/G1 arrest and downregulates thymidylate synthase in colorectal cancer. Cancer letters. 2016; 373:227-233.
19. Conteas CN, Panossian AM, Tran TT, and Singh HM. Treatment of HIV-associated diarrhea with curcumin. Digestive diseases and sciences. 2009; 54:2188-2191.
20. Zhu DJ, Chen XW, Wang JZ, Ju YL, Ou Yang MZ, and Zhang WJ. Proteomic analysis identifies proteins associated with curcumin-enhancing efficacy of irinotecan-induced apoptosis of colorectal cancer LOVO cell. International journal of clinical and experimental pathology. 2014; 7:1-15.
21. James MI, Iwuji C, Irving G, Karmokar A, Higgins JA, Griffin-Teal N, Thomas A, Greaves P, Cai H, Patel SR, Morgan B, Dennison A, et al. Curcumin inhibits cancer stem cell phenotypes in ex vivo models of colorectal liver metastases, and is clinically safe and tolerable in combination with FOLFOX chemotherapy. Cancer letters. 2015; 364:135-141.
22. Kim TH, Song J, Alcantara Llaguno SR, Murnan E, Liyanarachchi S, Palanichamy K, Yi JY, Viapiano MS, Nakano I, Yoon SO, Wu H, Parada LF, et al. Suppression of peroxiredoxin 4 in glioblastoma cells increases apoptosis and reduces tumor growth. PloS one. 2012; 7:e42818.
23. Cheng TC, Lu JF, Wang JS, Lin LJ, Kuo HI, and Chen BH. Antiproliferation effect and apoptosis mechanism

of prostate cancer cell PC-3 by flavonoids and saponins prepared from Gynostemma pentaphyllum. Journal of agricultural and food chemistry. 2011; 59:11319-11329.

24. Pongjit K, and Chanvorachote P. Caveolin-1 sensitizes cisplatin-induced lung cancer cell apoptosis via superoxide anion-dependent mechanism. Molecular and cellular biochemistry. 2011; 358:365-373.
25. Gangemi G, Gazzerro P, Fiore D, Proto MC, Butini S, Gemma S, Casagni A, Laezza C, Vitale M, Ligresti A, Di Marzo V, Zisterer DM, et al. PBOX-15 induces apoptosis and improves the efficacy of oxaliplatin in human colorectal cancer cell lines. European journal of pharmacology. 2013; 714:379-387.
26. Yang CL, Ma YG, Xue YX, Liu YY, Xie H, and Qiu GR. Curcumin induces small cell lung cancer NCI-H446 cell apoptosis via the reactive oxygen species-mediated mitochondrial pathway and not the cell death receptor pathway. DNA and cell biology. 2012; 31:139-150.
27. Ye M, Zhang J, Zhang J, Miao Q, Yao L, and Zhang J. Curcumin promotes apoptosis by activating the p53-miR-192-5p/215-XIAP pathway in non-small cell lung cancer. Cancer letters. 2015; 357:196-205.
28. Kizhakkayil J, Thayyullathil F, Chathoth S, Hago A, Patel M, and Galadari S. Glutathione regulates caspase-dependent ceramide production and curcumin-induced apoptosis in human leukemic cells. Free radical biology & medicine. 2012; 52:1854-1864.
29. Ikuno N, Soda H, Watanabe M, and Oka M. Irinotecan (CPT-11) and characteristic mucosal changes in the mouse ileum and cecum. Journal of the National Cancer Institute. 1995; 87:1876-1883.
30. Chen S, Yueh MF, Bigo C, Barbier O, Wang K, Karin M, Nguyen N, and Tukey RH. Intestinal glucuronidation protects against chemotherapy-induced toxicity by irinotecan (CPT-11). Proceedings of the National Academy of Sciences of the United States of America. 2013; 110:19143-19148.
31. Wessner B, Strasser EM, Koitz N, Schmuckenschlager C, Unger-Manhart N, and Roth E. Green tea polyphenol administration partly ameliorates chemotherapy-induced side effects in the small intestine of mice. The Journal of nutrition. 2007; 137:634-640.
32. Tam ZY, Gruber J, Halliwell B, and Gunawan R. Context-Dependent Role of Mitochondrial Fusion-Fission in Clonal Expansion of mtDNA Mutations. PLoS computational biology. 2015; 11:e1004183.
33. Dorn GW, 2nd, and Kitsis RN. The mitochondrial dynamism-mitophagy-cell death interactome: multiple roles performed by members of a mitochondrial molecular ensemble. Circulation research. 2015; 116:167-182.
34. Zungu M, Schisler J, and Willis MS. All the little pieces. -Regulation of mitochondrial fusion and fission by ubiquitin and small ubiquitin-like modifer and their potential relevance in the heart. Circulation journal. 2011; 75:2513-2521.
35. Yoon YS, Yoon DS, Lim IK, Yoon SH, Chung HY, Rojo M, Malka F, Jou MJ, Martinou JC, and Yoon G. Formation of elongated giant mitochondria in DFO-induced cellular senescence: involvement of enhanced fusion process through modulation of Fis1. Journal of cellular physiology. 2006; 209:468-480.
36. Soto-Urquieta MG, Lopez-Briones S, Perez-Vazquez V, Saavedra-Molina A, Gonzalez-Hernandez GA, and Ramirez-Emiliano J. Curcumin restores mitochondrial functions and decreases lipid peroxidation in liver and kidneys of diabetic db/db mice. Biological research. 2014; 47:74.
37. Kaur H, Bal A, and Sandhir R. Curcumin supplementation improves mitochondrial and behavioral deficits in experimental model of chronic epilepsy. Pharmacology, biochemistry, and behavior. 2014; 125:55-64.
38. Kumar A, and Singh A. A review on mitochondrial restorative mechanism of antioxidants in Alzheimer's disease and other neurological conditions. Frontiers in pharmacology. 2015; 6:206.
39. Sastre-Serra J, Valle A, Company MM, Garau I, Oliver J, and Roca P. Estrogen down-regulates uncoupling proteins and increases oxidative stress in breast cancer. Free radical biology & medicine. 2010; 48:506-512.
40. Gibson RJ, Bowen JM, Inglis MR, Cummins AG, and Keefe DM. Irinotecan causes severe small intestinal damage, as well as colonic damage, in the rat with implanted breast cancer. Journal of gastroenterology and hepatology. 2003; 18:1095-1100.
41. Wang D, Tian M, Qi Y, Chen G, Xu L, Zou X, Wang K, Dong H, and Lu F. Jinlida granule inhibits palmitic acid induced-intracellular lipid accumulation and enhances autophagy in NIT-1 pancreatic beta cells through AMPK activation. Journal of ethnopharmacology. 2015; 161:99-107.
42. Chu C, Abbara C, Tandia M, Polrot M, Gonin P, Farinotti R, and Bonhomme-Faivre L. Cetuximab increases concentrations of irinotecan and of its active metabolite SN-38 in plasma and tumour of human colorectal carcinoma-bearing mice. Fundamental & clinical pharmacology. 2014; 28:652-660.